JAMES | Journal of Advances in Modeling Earth Systems

RESEARCH ARTICLE
10.1029/2018MS001512

Three-Moment Representation of Rain in a Bulk Microphysics Model

M. Paukert[1], J. Fan[1], P. J. Rasch[1], H. Morrison[2], J. A. Milbrandt[3], J. Shpund[4], and A. Khain[4]

[1]Pacific Northwest National Laboratory, Richland, WA, USA, [2]National Center for Atmospheric Research, Boulder, CO, USA, [3]Meteorological Research Branch, Environment and Climate Change Canada, Dorval, Quebec, Canada, [4]Department of Atmospheric Sciences, Hebrew University of Jerusalem, Jerusalem, Israel

Key Points:
- The three-moment rain scheme yields highly improved simulations of precipitation, compared to the original two-moment representation
- The relative contributions of sedimentation, evaporation, and breakup to the shapes of drop size distributions depend on the rain regime
- A new parameterization of self-collection and breakup based on lookup tables yields drop mean sizes comparable to a spectral bin scheme

Correspondence to:
M. Paukert and J. Fan,
marco.paukert@pnnl.gov;
jiwen.fan@pnnl.gov

Citation:
Paukert, M., Fan, J., Rasch, P. J., Morrison, H., Milbrandt, J. A., Shpund, J., & Khain, A. (2019). Three-moment representation of rain in a bulk microphysics model. *Journal of Advances in Modeling Earth Systems*, *11*. https://doi.org/10.1029/2018MS001512

Received 24 SEP 2018
Accepted 16 DEC 2018
Accepted article online 19 DEC 2018

Abstract A bulk three-moment representation for rain microphysics is developed and implemented in the Predicted Particle Properties (P3) microphysics scheme. In addition, a new parameterization for rain self-collection and collisional breakup (RSCB) is presented using a lookup table approach, based on the Spectral-Bin Model (SBM). To quantify the impacts of sedimentation, evaporation, and RSCB on drop size distributions (DSDs), a rain shaft model is applied to a wide range of atmospheric scenarios (i.e., initial conditions and regimes) and compared against results from the SBM. DSD shapes are mainly determined by both sedimentation and evaporation, except in heavy rain where the impact of RSCB on DSD shape becomes more important than evaporation. The new parameterization for RSCB has a considerable impact on the mean drop size, improving the agreement between P3 and SBM. Only 4% of the original two-moment rainshaft simulations have mean drop sizes and rain rates within ±20% of the SBM results, but this increases to more than 95% agreement when the three-moment rain representation is used together with the new parameterization for RSCB. Generally, the improvement is more significant for heavy rain than for light drizzle. Remaining differences between bin and bulk model are attributable to treatments of evaporation, and the restriction to gamma DSDs in P3.

Plain Language Summary We improve the representation of rain for numerical models of the atmosphere. This is achieved by adding an additional predicted variable to allow for a more physically based prediction of raindrop sizes evolving from various microphysical processes, such as gravitational settling, evaporation, and growth and breakup upon drop-drop collisions.

1. Introduction

Clouds modulate atmospheric radiation and regulate the hydrological cycle, while latent heating and cooling associated with cloud hydrometeors impact the atmospheric circulation. Raindrops play a major role in the vertical redistribution of heat and moisture, and thus, to understand weather and climate, the physics of rain deserves careful consideration. However, representing clouds and precipitation in weather and climate models has been challenging (e.g., Forbes et al., 2015).

Rain is characterized fundamentally by drop size distributions (DSDs). The ability to describe DSDs using analytic functions is useful not only from a modeling perspective but also for remote sensing applications. Marshall and Palmer (1948) described DSDs using exponential functions of the drop diameter. Ulbrich (1983) established that DSDs can be better approximated by a three-parameter gamma distribution. While it encompasses the special case of an exponential distribution, the additional degree of freedom is also able to capture the varying shapes of rain DSDs found in nature, as well as features like decreasing concentrations toward the smallest drop sizes.

Observational studies have relied on gamma DSDs extensively (e.g., Bringi et al., 2003; Ulbrich & Atlas, 2007; Waugh et al., 2018). By analyzing long-term disdrometer data collected in 12 different locations, Dolan et al. (2018) found a clustering of DSD properties within the space of gamma DSD characteristics, representative of various rain regimes. Overall, these findings imply that a better representation of DSDs in models requires careful consideration of the physical processes within and below clouds. A computationally efficient yet physically based method to represent microphysics is the bulk approach, which predicts one or more moments of the DSD, which can be mapped to the parameters of the gamma

distribution. In line with observed rain properties, a popular choice is the three-parameter gamma distribution,

$$f(D) = N_0 D^{\mu} e^{-\lambda D} \tag{1}$$

where D is the diameter, N_0 is the intercept parameter, μ is the shape parameter, and λ represents the slope of the distribution. In a direct comparison with beta and log-normal distributions, Ziemer and Wacker (2014) concluded that the gamma distribution performs best in simulations of pure sedimentation.

In the widely used two-moment approach for bulk microphysics schemes (e.g., Khain et al., 2015; Lim & Hong, 2010; Milbrandt & Yau, 2005a; Morrison et al., 2009; Seifert & Beheng, 2006), the zeroth and third moments (M_0, M_3) of $f(D)$ are predicted. Usually, the values of the intercept and slope parameters of the DSD are calculated based on M_0 and M_3, while the shape parameter μ is still undetermined. Without explicit knowledge, a plausible approach is to assume the gamma distribution reduces to the exponential distribution ($\mu = 0$; e.g., Morrison et al., 2005), in line with some observations as well as earlier cloud models (e.g., Lin et al., 1983; Wisner et al., 1972). However, a basic problem of constant $\mu = 0$ is excessive size sorting (e.g., Milbrandt & McTaggart-Cowan, 2010; Shipway & Hill, 2012; Wacker & Seifert, 2001). Size sorting occurs in a population of different-sized drops when larger drops sediment faster than smaller ones, resulting in their spatial separation. In two-moment bulk schemes, this is achieved by separately applying number-weighted and mass-weighted mean fall speeds to sediment M_0 and M_3, respectively. Physically, the DSD should become narrower as a result of this separation. This should limit further size sorting because the mass- and number-weighted fall speeds for a narrow DSD (i.e., with large μ) are closer to one another than they are for a wide DSD (i.e., with μ near 0). This feedback between the shape parameter and weighted fall speeds cannot be represented in a model when μ is constant. Consequently, the leading edge of precipitation in particular has mean drop sizes too large in two-moment schemes with constant $\mu = 0$ (Wacker & Seifert, 2001), which affects not only the precipitation flux directly but also the efficiency of evaporation and collisional growth.

Instead of assuming a constant shape parameter, attempts have been made to diagnose μ. Statistical analyses of observed DSDs suggested that the three parameters of the DSD may not be completely independent of one another (e.g., Ulbrich, 1983), thus reducing the number of degrees of freedom. Relationships have been proposed between shape and slope, inferred from both disdrometer and radar observations (e.g., Brandes et al., 2003; Cao et al., 2008; G. Zhang et al., 2001). It was shown that such relationships can reasonably approximate DSDs for some rain regimes; however, they were less accurate more generally across multiple regimes (Seifert, 2005). Atlas and Ulbrich (2006) found that the μ-λ relationship varied even for a single storm passing over a measurement site, associated with convective, transition, and stratiform rain regions. Another approach for deriving diagnostic parameterizations of μ for two-moment schemes is to use bin microphysical models that explicitly evolve DSDs (Milbrandt & Yau, 2005a; Seifert, 2008). However, recent comparison between explicitly simulated and diagnosed DSD shapes supports the notion that diagnostic μ relationships depend on the rain regime (Naumann & Seifert, 2016).

To allow for a physically based evolution of DSD shapes, three-moment bulk schemes were developed in which an additional moment (usually the sixth moment, M_6, proportional to radar reflectivity for constant-density spherical particles) was added to predict μ (Milbrandt & Yau, 2005b, MY05b hereafter; Dawson et al., 2014; Loftus et al., 2014; Naumann & Seifert, 2016; Shipway & Hill, 2012; Szyrmer et al., 2005). MY05b first developed a three-moment representation for all hydrometeor classes, including both liquid and ice particles. The primary physical process considered for predicted shape parameters was the effect of sedimentation, thereby mitigating the problem of excessive gravitational size sorting. For processes other than sedimentation, approximate relations were introduced to enable the budgeting of M_6. Naumann and Seifert (2016) recently developed more detailed formulations of such processes for the budget of M_6 in their three-moment rain scheme, including evaporation and collision-coalescence. Using a Lagrangian drop model as a reference, they showed good agreement with their three-moment scheme. According to observations, model simulations and theory, rain self-collection and collisional breakup (hereafter *RSCB*) in heavy rain are expected to contribute significantly to the modification of DSD shapes (Hu & Srivastava, 1995; List & McFarquhar, 1990; Ulbrich, 1983). To date, breakup of raindrops has not been considered explicitly in three-moment bulk schemes. While sedimentation alone creates narrow DSDs, both evaporation and RSCB should counteract this tendency to some extent.

A recently developed two-moment microphysics model is the Predicted Particle Properties (P3) scheme (Morrison & Milbrandt, 2015, MM15 hereafter; Milbrandt & Morrison, 2016). P3 offers a new approach to representing the evolution of ice particles that is more physical than the traditional approach of using predefined ice categories. The reduced number of prognostic variables also makes its computational cost somewhat cheaper than many traditional schemes (Morrison et al., 2015). Both of these benefits make it a suitable choice for cloud-resolving and next-generation Earth system models. Our ultimate goal is to apply a full three-moment version of P3 to the U.S. Department of Energy's Energy Exascale Earth System Model (E3SM; K. Zhang et al., 2018; S. Xie et al., 2018). Toward this end, we focus on the development of three-moment rain microphysics; work is also underway to develop a three-moment representation for ice in P3 that will be reported on in a future publication.

In the current study, we implement an additional prognostic moment of the rain DSD (M_6) in P3 to replace the empirical shape-slope relation based on Cao et al. (2008). A unique feature of our implementation compared to existing three-moment schemes is the explicit consideration of RSCB on the DSD shape. This is achieved by using the Spectral-Bin Model (SBM; Khain et al., 2004) to create lookup tables with dependencies on the DSD properties. Based on the new approach, we also address the question: is it important to consider the impacts of evaporation and RSCB on DSD shapes? This is done using a one-dimensional rainshaft model run over a wide variety of rain regimes.

The remainder of this paper is structured as follows. Section 2 is dedicated to the model implementation of the three-moment scheme. Section 3 describes the model setup of the rainshaft simulations, and in section 4 we present the corresponding results. Section 5 summarizes and concludes the paper. Appendices A–C contain information on the lookup tables of RSCB, the calculation of mean sizes, and a list of symbols, respectively.

2. Development of Three-Moment Rain Microphysics

In line with MM15, here we call any advected model tracers *prognostic* variables, whereas a property calculated as a function of the prognostic variables is *predicted* in that it is a completely free parameter. In the two-moment P3 we call μ *diagnosed* on the basis of an empirical relation. Although the outcome of μ is also the result of the prognostic variables M_0 and M_3 in two-moment scheme, to enable the diagnosis of three parameters from the two moments requires an additional relation or assumption. A list of symbols is included in Appendix C.

Like in existing three-moment schemes (e.g., MY05b), the prognostic variables used in our implementation are moments M_0, M_3, and M_6. Morrison et al. (2016) show that numerical artifacts due to advection can have considerable impacts on predicted quantities that are calculated from the combination of multiple prognostic variables. They proposed that such artifacts can be limited if the set of prognostic variables is chosen in a way that allows calculating the predicted variable as a ratio of the prognostic quantities. For the three-moment scheme, we choose to advect $\mathrm{SQNZ} = (N_r\, M_6)^{0.5}$ rather than M_6, where N_r is the number mixing ratio of rain. SQNZ has units of m^3/kg and is conserved during three-dimensional advection. In this approach, the shape is a function of the ratio SQNZ/q_r (see below, equation (2)), where q_r is the mass mixing ratio of rain. SQNZ is converted to M_6 for the use within the microphysics scheme. While the diagnosed shape parameter in the two-moment P3 yields maximum μ values of approximately 8.3, we allow for predicted values up to 20. The lower limit is 0, representative of an exponential distribution.

With our choice of prognostic moments the basic principles are similar to MY05b; therefore, we focus on details of the implementation that are specific to the P3 scheme. Note that here we use mixing ratios rather than densities in contrast to MY05b. Thus, in the following, (bulk) mass and (bulk) number refers to mass and number mixing ratios, respectively. Generally in bulk schemes, it is assumed that the DSD covers all sizes from zero to infinite diameters. Within clouds, this treatment implies overlapping size distributions of cloud droplets and raindrops. Below clouds, it is reasonable to allow for the presence of small raindrops in the DSD spectrum because evaporation leads to a continuous shrinking of drops.

The main purpose of the three-moment scheme is to obtain the DSD shape as a function of the moments. With $c = \rho_w\, \pi/6$, it follows $q_r = c\, M_3$. Using the analytic expression of the kth moment of the gamma DSD, $M_k = N_r/\lambda^k\, \Gamma(\mu + 1 + k)/\Gamma(\mu + 1)$, the dimensionless ratio of the three predicted

moments (equation (2)) can be rewritten to obtain a cubic equation with coefficients c_1, c_2, and c_3 (equation (3)) depending on the prognostic variables N_r, q_r and M_6 (equation (4)):

$$\frac{M_0 M_6}{M_3^2} = \frac{(\mu+6)(\mu+5)(\mu+4)}{(\mu+3)(\mu+2)(\mu+1)} = c^2 \frac{N_r\, M_6}{q_r^2} = K \tag{2}$$

$$\mu^3 + c_1\,\mu^2 + c_2\,\mu + c_3 = 0 \tag{3}$$

$$c_1 = \frac{15-6K}{1-K}; \quad c_2 = \frac{74-11K}{1-K}; \quad c_3 = \frac{120-6K}{1-K}; \tag{4}$$

For $\mu \geq 0$ relevant to our scheme, equation (3) has a single unique solution. For $K > 20$ ($K < 1.46$), we set $\mu = 0$ ($\mu = 20$) as a lower (upper) limit to the shape. Otherwise, equation (3) is solved following Press et al. (1992, pp. 179–180). For a physically based prediction of the moments used in equation (2), the microphysical process rates are calculated as described in the following.

2.1. Rain Self-Collection and Collisional Breakup

A new parameterization for the process rates of bulk number and M_6 from RSCB is derived. We use a lookup table approach with dependencies on all three parameters of the gamma distribution. This is achieved by creating two-dimensional lookup tables with dimensions of shape parameter μ and the number-weighted mean size D_n (equation (B2)). Although the tables have two dimensions, using a DSD scaling approach yields the additional, third dependency. Quantities used by the scheme, denoted as $\text{table}_{Nr}(\mu, D_n)$ for bulk number and $\text{table}_{M6}(\mu, D_n)$ for the sixth moment, are obtained from two-dimensional linear interpolation of the lookup table values. The process rate is then obtained by rescaling these interpolated quantities using the factor $f_{\text{scale}} = (\rho_{\text{air}} N_r/\Gamma(\mu + 1))^2$ (equation (A3)), for example, for the change in bulk number from RSCB:

$$\frac{dN_r}{dt} = \frac{f_{\text{scale}}}{\rho_{\text{air}}}\ \text{table}_{Nr}(\mu, D_n) \tag{5}$$

with ρ_{air} representing the local air density needed to convert from a concentration tendency in the lookup table to a mixing ratio tendency in P3. μ, D_n, and N_r represent the local rain properties in each grid box. In two-moment configurations, only one table is necessary to predict the number rate, while in the three-moment scheme an additional table for M_6 accounts for the influence of RSCB on the DSD shape. The lookup table values are based on the spectral bin model (SBM; Shpund et al., Simulating Deep Convection and Mesoscale Phenomena using WRF with Spectral Bin Microphysics - Part 1: Dominating Hydrometeor Type, to be submitted), which was updated based on Khain et al. (2004). The approach is further described in Appendix A.

2.2. Sedimentation

In our three-moment implementation, we calculate the moment-weighted mean fall speeds V_0, V_3, and V_6, defined by

$$V_k = \frac{\int v(D)\, D^k\, f(D)\, \mathrm{d}D}{\int D^k\, f(D)\, \mathrm{d}D} \tag{6}$$

where $v(D)$ is the fall speed of a drop with diameter D and k is equal to 0, 3, or 6. The size-dependent fall speed of raindrops in P3 is approximated by three power laws for three size intervals of the DSD (Appendix A of MM15). By numerically integrating the size distribution, the mean fall speeds are precalculated once and stored in lookup tables that depend on the DSD properties, which means that computationally costly incomplete gamma functions do not have to be calculated at runtime. The default two-moment version of P3 used this approach to obtain V_0 and V_3, and for the three-moment approach here we extend this to include tabulated values for V_6.

The influence of air density on fall speeds is considered by a multiplicative factor as described by MM15. Using these values of V_k, the vertical flux divergence yields the local rate of change of each prognostic moment from sedimentation.

2.3. Condensation and Evaporation

The budget of M_6 due to condensation and evaporation includes two contributions by (a) gain or loss of mass and (b) droplet depletion upon complete evaporation. The calculation in P3 is based on the supersaturation relaxation approach described in detail by Morrison and Grabowski (2008; MG08 hereafter) and MM15. Analogous to both equation (9) and equation (A5) of MG08, we obtain the bulk rate of M_6 by computing the expression

$$\frac{\mathrm{d}M_6}{\mathrm{d}t} = \frac{\overline{\delta}}{f_p} \frac{24\,\rho_{\mathrm{air}}\,D_v}{\rho_w} \int N_0\, D^{\mu+4} e^{-\lambda D} f_v(D)\,\mathrm{d}D \tag{7}$$

where $\overline{\delta}$ is the time step-averaged absolute supersaturation, f_p is the psychrometric factor, accounting for latent heating (denoted as Γ in equation (A4) of MG08), ρ_w is the density of liquid water, ρ_{air} the density of air, and D_v the diffusivity of water vapor. f_v is the size-dependent ventilation factor for a sedimenting drop, depending on drop fall speed $v(D)$. As in the case of sedimentation (equation (6)), three separate power laws for $v(D)$ make it convenient to precalculate part of the integral numerically and store the result in a lookup table, depending on the DSD properties. Overall, we get

$$\frac{\mathrm{d}M_6}{\mathrm{d}t} = \frac{\overline{\delta}}{f_p} \frac{24\,\rho_{\mathrm{air}}\,D_v}{\rho_w} \frac{N_r}{\Gamma(\mu+1)} \left(\frac{\Gamma(\mu+5)}{\lambda^4}\, 0.78 + 0.32\, Sc^{\frac{1}{3}} \left(\frac{\rho_{\mathrm{air}}}{\mu_{\mathrm{air}}}\right)^{\frac{1}{2}} \left[\lambda^{\mu+1} \int D^{\mu+4}\, e^{-\lambda D} (D\, v(D))^{\frac{1}{2}}\, \mathrm{d}D \right] \right) \tag{8}$$

where the expression in squared brackets is precalculated and stored in the lookup table. Sc is the Schmidt number, and μ_{air} the dynamic viscosity of air.

In case of evaporation, the fractional loss of bulk mass translates into a fractional loss of bulk number, assuming that the mean volume diameter MVD (equation (B1)) is maintained, that is, the ratio of q_r and N_r is constant during evaporation. This assumption is commonly used in bulk microphysical schemes, although Seifert (2008) discussed potential problems associated with it. Here we do not modify the original treatment in P3 based on this assumption, but its impact is further explored in section 4. While bulk mass loss is considered by equation (8), an additional contribution to the budget of M_6 is required to account for depleted droplets in the three-moment scheme. This is achieved by assuming that μ remains constant due to the sole action of depletion of the smallest raindrops. Therefore, in addition to equation (8) we add the tendency

$$\frac{\mathrm{d}M_6}{\mathrm{d}t} = -\frac{(\mu+6)(\mu+5)(\mu+4)}{(\mu+3)(\mu+2)(\mu+1)} \frac{1}{c^2} \left(\frac{q_r}{N_r}\right)^2 \frac{\mathrm{d}N_r}{\mathrm{d}t} \tag{9}$$

which is based on equation (2) of MY05b (see also below, equation (11)). The coefficient $c = \rho_w\,\pi/6$ originates from the mass-diameter relation $m = cD^d$. Although the aforementioned assumption is a simplification, sensitivity tests using the rain shaft model (setup as described in section 3) confirm that using equation (9) in addition to equation (8) yields a clearly better match between the predicted DSD shape in the three-moment scheme and the bin model compared to neglecting the contribution of equation (9), which yields too narrow DSDs (not shown).

2.4. Other Processes Affecting M_6

A number of processes rely on the closure assumptions discussed in MY05b. These include rain initiation by autoconversion and rain growth by accretion of cloud droplets. While in the current study, we focus on warm processes, in mixed-phase cloud regimes, freezing, riming, shedding, and melting also need to be considered.

For autoconversion and shedding, the size distribution of newly created droplets has a constant, predefined width, $\mu_{\mathrm{init}} = 2$ (MY05b). Thus, the rate of M_6 can be inferred from equation (4) of MY05b:

Table 1
Overview of the 450 Scenarios Simulated in the Rainshaft Model

Symbol	Description	Values
RH_{init}	Column relative humidity (%)	30, 50, 70, 90, 95
z_{init}	Column height (m)	500, 1500, 4500
$q_{r,\ init}$	Initial rain bulk mass (g/kg) (mean volume diameter, μm)[a]	0.1, 0.3, 1.0, 3.0, 6.0 (267, 386, 576, 830, 1,046)
μ_{init}	Initial rain shape parameter	0, 1, 5
$\tau_{T,\ RH}$	Nudging time scale for T and RH (min)	15, 60

Note. RH = relative humidity.
[a]The mean volume diameter is the result of $q_{r,\ init}$ and initialized bulk rain number of 10^4 kg^{-1}, the latter being the same in all simulations.

$$\frac{dM_6}{dt} = \frac{(\mu_{init}+6)(\mu_{init}+5)(\mu_{init}+4)}{(\mu_{init}+3)(\mu_{init}+2)(\mu_{init}+1)} \frac{1}{c^2} \left(\frac{dq_r}{dt}\right)^2 \left(\frac{dN_r}{dt}\right)^{-1} \quad (10)$$

For accretion (rain collecting cloud droplets), freezing, riming, and melting, it is assumed that μ remains constant during these processes. Accordingly, we use equation (2) of MY05b:

$$\frac{dM_6}{dt} = \frac{(\mu+6)(\mu+5)(\mu+4)}{(\mu+3)(\mu+2)(\mu+1)} \frac{1}{c^2} \left[2\frac{q_r}{N_r}\frac{dq_r}{dt} - \left(\frac{q_r}{N_r}\right)^2 \frac{dN_r}{dt}\right] \quad (11)$$

We note that the treatment of melting as described above may be considered preliminary and will be further discussed in future studies of deep convective clouds.

3. Rainshaft Model Setup

One-dimensional (1-D) models are a useful tool to evaluate new model developments (e.g., Brdar & Seifert, 2018; Chosson et al., 2014; Milbrandt & Morrison, 2016) and provide physical insight into microphysical processes (e.g., Kumjian & Ryzhkov, 2010) needed to develop new parameterizations (e.g., Seifert, 2008, and references therein).

The 1-D kinematic driver model from Milbrandt et al. (2012) is used here. The model consists of 41 vertical levels which extend up to 12.8 km with a vertical grid spacing between 35 and 345 m at the relevant altitudes. The time step is 10 s, comparable to cloud-resolving models. The model was extended to drive both the SBM and P3 schemes. With each of the 10 microphysics model configurations described below, we conduct 450 simulations with varying conditions of initial rain height (z_{init}), rain mass mixing ratio ($q_{r,\ init}$), DSD shape (μ_{init}), relative humidity (RH_{init}), and environmental forcing ($\tau_{T,\ RH}$). The specified values are summarized in Table 1.

Rain microphysical processes considered in the simulations include sedimentation, evaporation, and RSCB. With a focus on subcloud processes, we specify the initial rain properties at altitude z_{init}, rather than allowing collision-coalescence to form rain as the latter is known to be different between bin and bulk models. To address the sensitivity to initial rain properties, we vary both the initial bulk mass ($q_{r,\ init}$) and shape parameters (μ_{init}). Furthermore, we vary the precipitation depth by specifying three different values of z_{init}. The initial atmospheric temperature profile is characterized by a surface temperature of 30 °C to allow for nonfreezing temperatures in case of the highest z_{init}, and a constant vertical temperature gradient of 6.5 K/km. The initial water vapor profile is specified to yield a vertically constant RH between 30% and 95%.

In reality, both temperature and humidity may evolve depending on the microphysics, for example, evaporation. Advection of temperature and humidity as well as turbulent mixing would tend to maintain the vertical profiles, keeping the thermodynamic properties similar to the environment. To account for this, we allow feedback between the microphysics and temperature and water profiles but use a relaxation approach to keep these profiles close to the initial values. Two nudging time scales ($\tau_{T,\ RH}$) are applied in order to mimic different environments, given by temperature and humidity profiles. The approach is implemented in the model by adding a source term, for example, for temperature $dT/dt = (T_0 - T)/\tau_{T,\ RH}$, where T_0 is the specified initial profile, T is the actual temperature, and dt is the model time step. This approach yields an increasing relative humidity with height, that is, the simulated environment is moister than RH_{init}. Three hour simulations are performed with the rain properties at z_{init} held constant, to arrive near a steady state. The analysis is restricted to rain properties in the steady state. Instead of applying the relaxation approach for the temperature and humidity profiles, we also ran simulations in which temperature and humidity were held constant in time (results not included in this paper). However, these results do not affect the overall conclusions described in this paper. An example of the time evolution of temperature and humidity depending on $\tau_{T,\ RH}$ is given in Figure 1.

Table 2 summarizes the various configurations of P3 and SBM that are compared in the rain shaft simulations. In the default two-moment P3 scheme (2m-C08-SBV), the DSD shape parameter is a function of

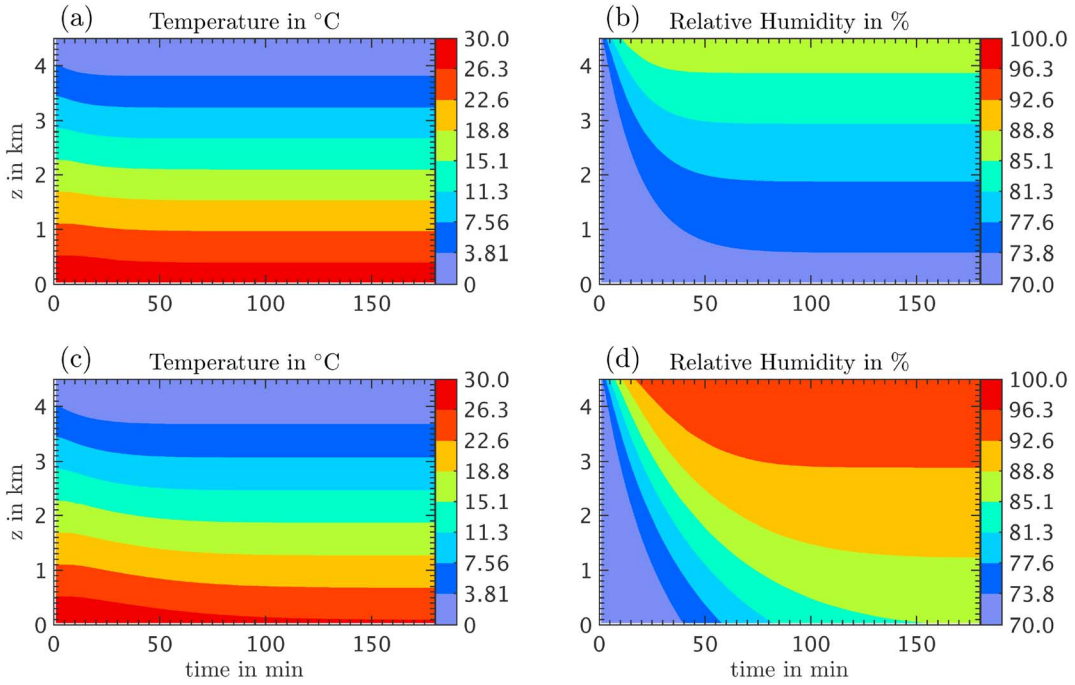

Figure 1. Time evolution of temperature (a, c) and relative humidity (b, d) in the column simulated by the reference model (Spectral-Bin Model). The top row is for $\tau_{T,\ \mathrm{RH}} = 15$ min and the bottom row for $\tau_{T,\ \mathrm{RH}} = 60$ min. The initial conditions represent an example of intermediate values, with $\mathrm{RH}_{\mathrm{init}} = 70\%$, $q_{r,\ \mathrm{init}} = 1$ g/kg, $\mu_{\mathrm{init}} = 1$, and $z_{\mathrm{init}} = 4{,}500$ m.

DSD slope following Cao et al. (2008). To show its impact compared to a specified constant value, the 2m-μ0-SBV configuration uses a constant $\mu = 0$. Furthermore, the impact of the RSCB lookup table approach used in conjunction with the default treatment of the shape parameter is shown in case 2m-C08-TBL. In this configuration, the lookup table for the bulk number rate of RSCB replaces the self-collection parameterization (Seifert & Beheng, 2001) and the breakup scheme based on Verlinde and Cotton (1993; see Morrison et al., 2012) in the default two-moment P3.

For the three-moment simulations, the configurations 3m-S-SBV, 3m-SE-SBV, and 3m-full are run to test the impacts of sedimentation, evaporation, and RSCB on DSD shape. In order to explore the effect of the new RSCB parameterization, two additional configurations (3m-S-TBL and 3m-SE-TBL) are run in which the number rates of RSCB processes are calculated with the lookup table. In the configurations with semi-idealized treatments of the DSD shape (3m-S-SBV, 3m-SE-SBV, 3m-S-TBL, and 3m-SE-TBL), a subset

Table 2
Overview of Sensitivity Simulations Carried Out in the Rainshaft Model

Configuration	Description	RSCB treatment for bulk number[a]
SBM	Spectral-bin microphysics scheme	S05
SBM-Γ	SBM with DSDs forced to be gamma distributions at the end of each time step	S05
2m-μ0-SBV	Two-moment P3 with $\mu = 0$	SB01, VC93
2m-C08-SBV	Two-moment P3 with diagnosed μ (default P3, following Cao et al., 2008)	SB01, VC93
2m-C08-TBL	Two-moment P3 with diagnosed μ	$\mathrm{table}_{\mathrm{Nr}}$
3m-S-SBV	Three-moment P3 with sedimentation determining μ	SB01, VC93
3m-S-TBL	Three-moment P3 with sedimentation determining μ	$\mathrm{table}_{\mathrm{Nr}}$
3m-SE-SBV	Three-moment P3 with sedimentation and evaporation determining μ	SB01, VC93
3m-SE-TBL	Three-moment P3 with sedimentation and evaporation determining μ	$\mathrm{table}_{\mathrm{Nr}}$
3m-full	Three-moment P3 with sedimentation, evaporation and RSCB determining μ	$\mathrm{table}_{\mathrm{Nr}}$

Note. SBM = Spectral-Bin Model; RSCB = rain self-collection and collisional breakup; DSDs = drop size distributions.
[a]The treatments of RSCB parameterizations refer to the default implementations following Seifert et al. (2005; S05) in SBM, Seifert and Beheng (2001; SB01) in combination with Verlinde and Cotton (1993; VC93) in the original P3, and our lookup table approach based on SBM (section 2.1).

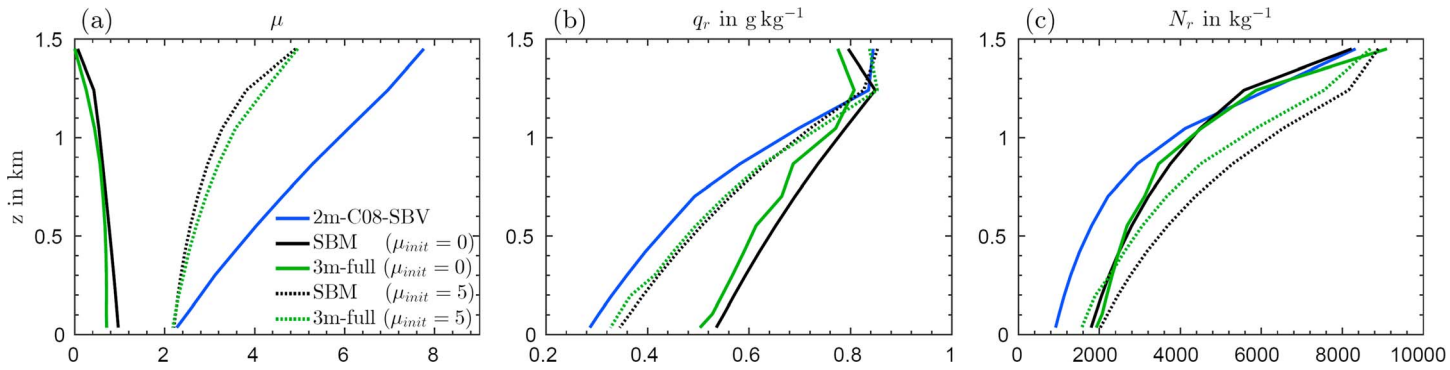

Figure 2. Profiles of (a) shape parameter, (b) rain mass mixing ratio, and (c) rain number mixing ratio after 180-min simulation time. Two scenarios are shown by solid lines ($\mu_{\text{init}} = 0$) and dotted lines ($\mu_{\text{init}} = 5$), both of which are based on $\text{RH}_{\text{init}} = 70\%$, $q_{r,\ \text{init}} = 1$ g/kg, $z_{init} = 1{,}500$ m, and $\tau_{T,\ \text{RH}} = 15$ min. The 2m-C08-SBV configuration is insensitive to the specified shape parameter so the solid and dotted lines overlap. The difference between initialized and plotted mass mixing ratios in the uppermost level in (b) reflects the loss from sedimentation and evaporation during one time step.

of processes does not contribute to the predicted shape. Specifically, neither evaporation nor RSCB influence μ in the 3m-S-SBV and 3m-S-TBL configurations. Thus, rates of M_6 for these processes are based on equation (11), corresponding to the treatments in MY05b. Similarly, RSCB does not influence μ in the 3m-SE-SBV and 3m-SE-TBL configurations (using equation (11)), while evaporation influences μ based on equations (8) and (9).

Results from the above two-moment and three-moment P3 configurations are compared with those from SBM, which serves as a benchmark. SBM-Γ is a sensitivity test based on SBM to estimate the impact of assuming a gamma drop size distribution, rather than allowing free evolution of the DSD. In each time step, all processes may modify the DSD without restrictions. However, at the end of each time step the binned DSD concentrations are redistributed in accordance with a gamma distribution, while DSD moments are conserved. This configuration might be interpreted as a bulk-emulating bin model, allowing us to isolate the effects of parameterization assumptions between the bin and bulk microphysics approaches. A similar approach was used by Igel and van den Heever (2017) in their *bin as bulk* simulations. The difference is that in SBM-Γ, the DSD shape is predicted (corresponding to a three-moment bulk scheme), rather than using a constant value for μ throughout the simulation (corresponding to a two-moment bulk scheme).

Comparing DSD properties between bulk and bin model requires defining which part of the spectrum is considered *rain* in SBM. In the rain shaft model, we define all drop sizes to be rain for two reasons, (a) for consistency with the assumptions made in the bulk scheme and (b) since we only initiate rain, it is reasonable to assume that partially-evaporating raindrops remain raindrops, that is, the smallest drops are not converted to cloud droplets.

4. Results

4.1. Overview of Model Performances

To gain understanding of the simulated profiles, we first show the results with intermediate initial conditions out of the 450 scenarios as an example in Figure 2. It is seen that the diagnosed DSDs in 2m-C08-SBV are narrower than those predicted in both SBM and 3m-full (Figure 2a). The difference between the profiles of μ in the two-moment and three-moment P3 is particularly pronounced when the initial DSDs are broad. The agreement of P3 with SBM-simulated profiles is much improved in the 3m-full configuration. Even though the low-level μ in 2m-C08-SBV agrees with the predicted values in case of $\mu_{\text{init}} = 5$, the discrepancy at upper levels is still important in determining surface rain properties. With too narrow DSDs in 2m-C08-SBV, mass is depleted too efficiently by evaporation (Figure 2b). Bulk number (Figure 2c) is influenced by both evaporation and RSCB. One aspect is that bulk number mixing ratios diverge between SBM and 3m-full, particularly in case of narrow DSDs, which will be further discussed in section 4.2.5.

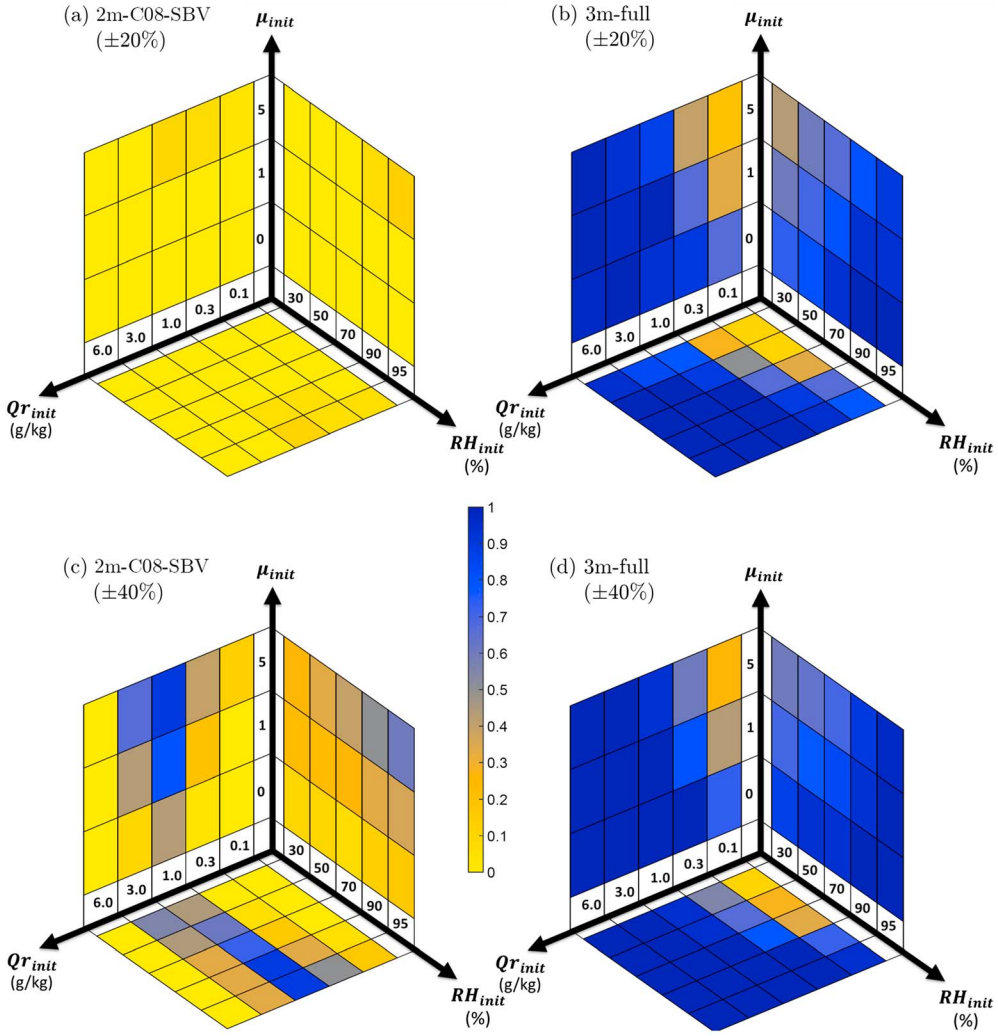

Figure 3. Model performance of the P3 scheme relative to SBM under different initial conditions: relative humidity (RH_{init}), shape parameter (μ_{init}), and rainwater mixing ratio (Qr_{init}). Colors indicate the fraction of P3 runs in which RR, MVD, and D_n are within ±20% compared to SBM (a, b), and within ±40% compared to SBM (c, d). The P3 configurations represent the default scheme 2m-C08-SBV (a, c) and the three-moment scheme 3m-full (b, d). In each two-dimensional plane, every cell represents the simulations initiated with the other three dimensions shown in Table 1 (e.g., in the plane of Qr_{init}-μ_{init}, there are 5 RH_{init}, 3 z_{init}, and 2 $\tau_{T,\ RH}$ values, which are $5 \times 3 \times 2 = 30$ simulations per cell). Each individual simulation either fulfills the joint requirements for RR, MVD, and D_n or not, and the fraction of positive outcomes is represented by colors. SBM = Spectral-Bin Model.

Next, we evaluate the scheme performance for the wide range of initial conditions. As a summary measure of performance, a simulation is considered similar to SBM when surface rain rate (RR), mean volume diameter (MVD), and number-weighted mean size (D_n) are within ±20% of the SBM values. These properties represent a summary of the final outcome of the microphysical processes within the simulated column. Two measures of the mean size are chosen: MVD as a function of bulk mass and number (equation (B1)), and D_n with the additional dependency on the shape (equation (B2)). We note that this measure of performance does not differentiate the individual simulations that are considerably better or considerably worse than the chosen threshold. A more quantitative analysis is presented in section 4.2.

A summary of the fidelity of P3 runs compared to SBM is displayed in Figure 3, partitioned by each run's initial values of relative humidity, shape parameter, and rainwater mixing ratio at the top of the rain shaft. In each cell in the figure, the fraction of runs considered similar to SBM is indicated by colors, with yellow (blue) colors indicating a poor (good) agreement with the SBM simulations. While Figures 3a and 3b use the

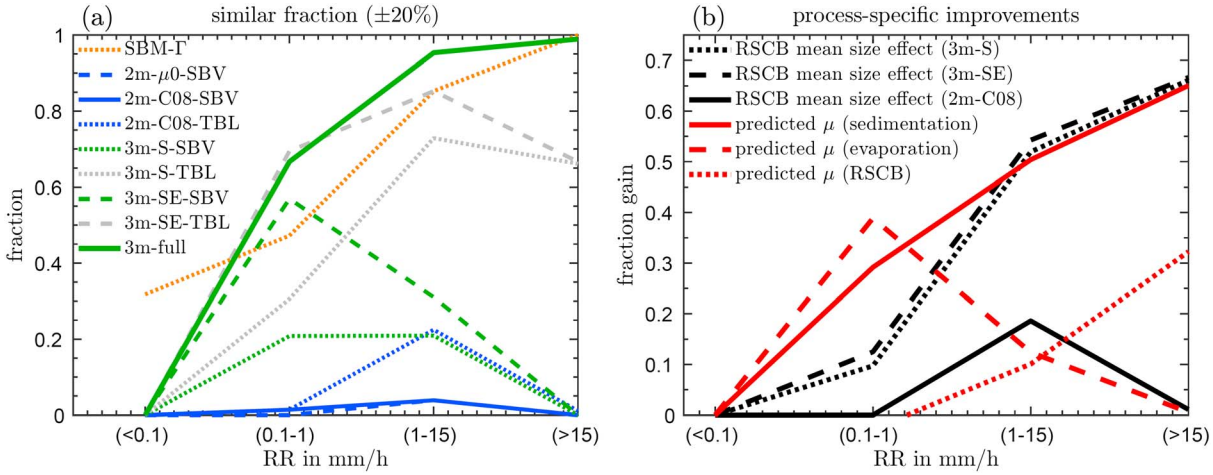

Figure 4. (a) Performance of the different microphysical configurations (see Table 2), indicated by the fraction of simulations that are similar to the SBM-simulated rain rates and mean sizes (±20% relative to SBM). The 450 scenarios are split into four regimes of surface rain intensity based on the SBM-simulated rain rates. (b) The fraction gain is the difference between pairs of lines from (a), representing the contribution of predicted shape due to different microphysical processes (red) and the mean size effect of RSCB lookup tables (black) to the improvements shown in (a). The legend names in (b) correspond to the *Description* column of Table 3, and the lines represent the difference between *Configuration 2* and *Configuration 1* shown in Table 3. The mean size effect refers to the impact of using the new RSCB parameterization to calculate bulk number rates due to RSCB. SBM = Spectral-Bin Model; RR = rain rate; RSCB = rain self-collection and collisional breakup.

aforementioned ±20% criterion for RR, MVD, and D_n, we also show results with a relaxed threshold of ±40% (Figures 3c and 3d) in order to better see the regime dependence of the two-moment scheme.

Few runs with the original P3 scheme (2m-C08-SBV) meet the ±20% criterion, as indicated by yellow colors in Figure 3a. With a relaxed criterion, 2m-C08-SBV shows some similarity to SBM for a narrow range of $q_{r,\,\mathrm{init}}$, around 1 g/kg, in conjunction with rather narrow initialized DSDs (large μ_{init}). The dependence on $\mathrm{RH}_{\mathrm{init}}$ indicates that in more humid atmospheres 2m-C08-SBV tends to be more similar to SBM than in dry atmospheres. The results of the new three-moment scheme (3m-full) are similar to those of SBM in the majority of scenarios, as indicated by blue colors in Figure 3b, except for conditions of small initial rain mass mixing ratios, dry environments, and narrow initial DSDs in which evaporation is dominant. As expected, the relaxed criteria of ±40% yields a slightly higher fraction of similar runs (Figure 3d). The dependence of model performance on z_{init} and $\tau_{T,\,\mathrm{RH}}$ is not shown explicitly in Figure 3. Generally, all P3 configurations tend to agree better with SBM when z_{init} is small (i.e., short sedimentation path), and when $\tau_{T,\,\mathrm{RH}}$ is large (i.e., weak coupling to the environmental conditions).

4.2. Microphysical Analysis and Sensitivity Studies

The following analysis provides understanding of (a) the properties of two- and three-moment configurations, (b) the processes that are most important for predicting the shape parameter, (c) the impact of RSCB treatments, (d) the potential limitation of a gamma size distribution, and (e) the role of evaporation in creating differences between P3 and SBM. Here we introduce the purpose of Figures 4–6, while the interpretation is presented in sections 4.2.1 to 4.2.5. In the discussion, surface rain intensities are classified as minor (RR < 0.1 mm/hr), light (0.1–1 mm/hr), intermediate (1–15 mm/hr), and heavy (RR > 15 mm/hr).

Figure 4a presents the performance for each microphysics configuration as a function of surface rain rate intensity (based on SBM-simulated rain), while Figure 4b identifies contributions of each process to the overall performance. Table 3 summarizes the configurations used to draw conclusions on the process contributions. Because the diagnosed contributions in Figure 4b depend on the simulation configurations chosen for comparison, it should not be interpreted as a strict ranking of the importance of processes. Our way of comparing simulations reflects the historical order of three-moment scheme developments, for example, the additional effect of evaporation builds upon a scheme that already considers size sorting. Likewise, quantification of the RSCB effect on the DSD shape is based on a configuration that considers the effects of

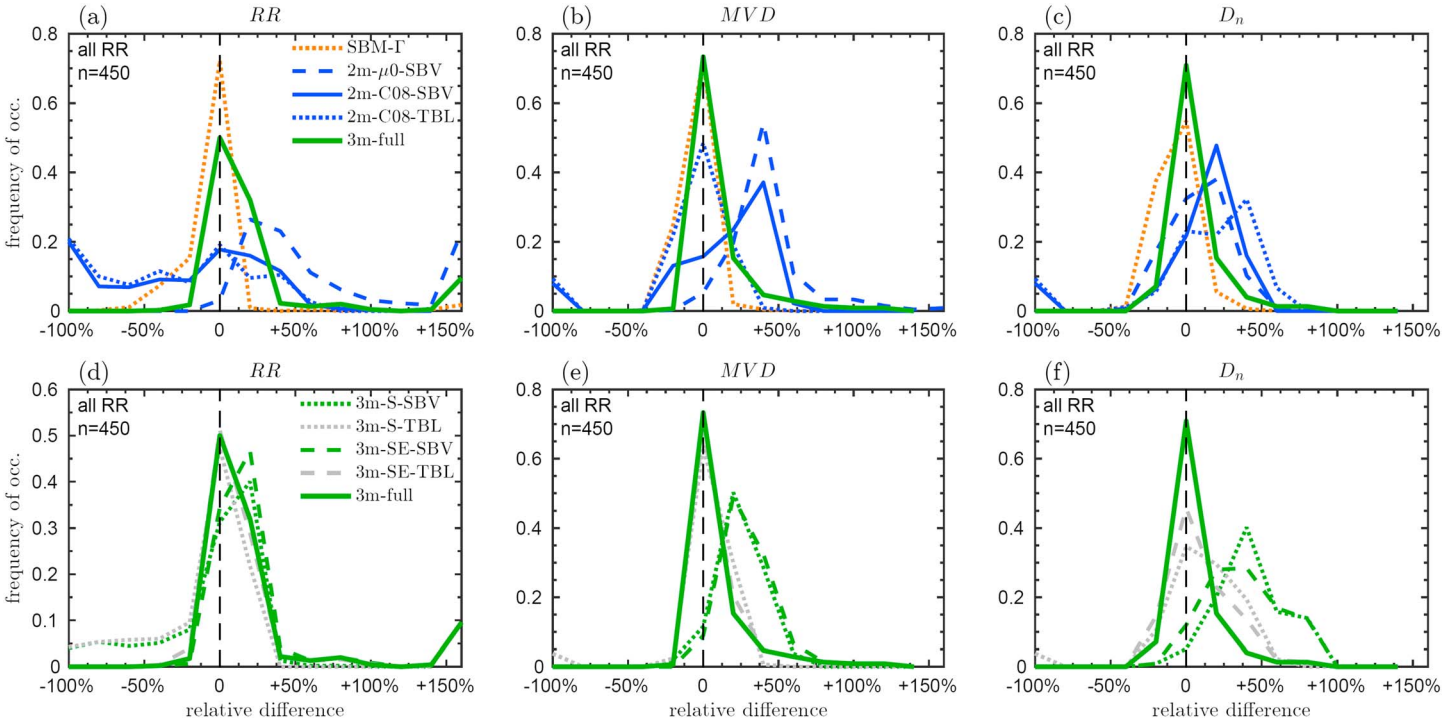

Figure 5. Occurrence frequencies of the relative deviation of the 450 simulations for each configuration compared to Spectral-Bin Model (SBM)-simulated rain rates (a, d), mean volume diameters (b, e), and number-weighted mean sizes (c, f), respectively. Upper and lower panels show the same information but for different microphysics configurations (3m-full is identical in upper and lower panels as a reference). Binning is done in 20% intervals, that is, the peaks centered at 0 contain all simulations within a ±10% relative error. All results with deviations larger than +150% are collected in the bin that is centered at +160%.

sedimentation and evaporation. Figure 5 characterizes deviations from the reference SBM solutions quantitatively in terms of occurrence frequencies of relative error in surface rain rates, MVD and D_n, all of which are considered in the performance criterion discussed above. In Figure 6 we further examine the biases in RR, q_r, N_r, MVD, μ, vertically integrated evaporation rates, and supersaturation with respect to water at the surface level ($s_w = q_v/q_{v,\,sat} - 1$). This analysis helps to identify the regimes associated with biases of rain properties in the default P3, and to pinpoint the reasons for differences between 3m-full and SBM-Γ. This will help to understand bin and bulk schemes and shed light on the potential for further improvements.

4.2.1. Diagnosed and Predicted Shape Parameters

Figure 4a shows that for RR < 0.1 mm/hr, none of the bulk P3 simulations meet the similarity criteria. For intermediate rain (1–15 mm/hr), the default P3 scheme (2m-C08-SBV) meets the criteria in about 4% of the simulations. The deviation of rain rate has a large scatter in both positive and negative directions (Figure 5a) and mean sizes are usually too large (Figures 5b and 5c). According to Figures 6a–6c, underpredicted rain rates in 2m-C08-SBV are mainly associated with RR < 15 mm/hr, and overprediction corresponds to RR > 15 mm/hr. In a number of two-moment simulations no precipitation arrives at the surface, indicated by the deviations of MVD and s_w equal to −100% and +100%, respectively (Figures 6k and 6t). The bias in RR can have two origins: (a) the direct influence of the DSD shape on the bulk fall speed and (b) the influence of the DSD shape on evaporation. For both, too narrow DSDs contribute to decreased surface precipitation, consistent with 2 m-C08-SBV (Figures 6n and 6o). When assuming a constant μ equal to zero (2m-μ0-SBV), the rain rates are exclusively overpredicted compared to SBM, with a significant fraction biased more than +150%, and MVDs being even larger than in 2m-C08-SBV (Figures 5a and 5b).

Major improvements are found by predicting the shape parameter in 3m-full relative to the two-moment configurations. The fraction of 3m-full simulations agreeing with SBM results within ±20% is more than 95% for intermediate and heavy rain regimes (Figure 4a). This is further confirmed in Figure 5, while three-moment configurations other than 3m-full are more likely to have biased

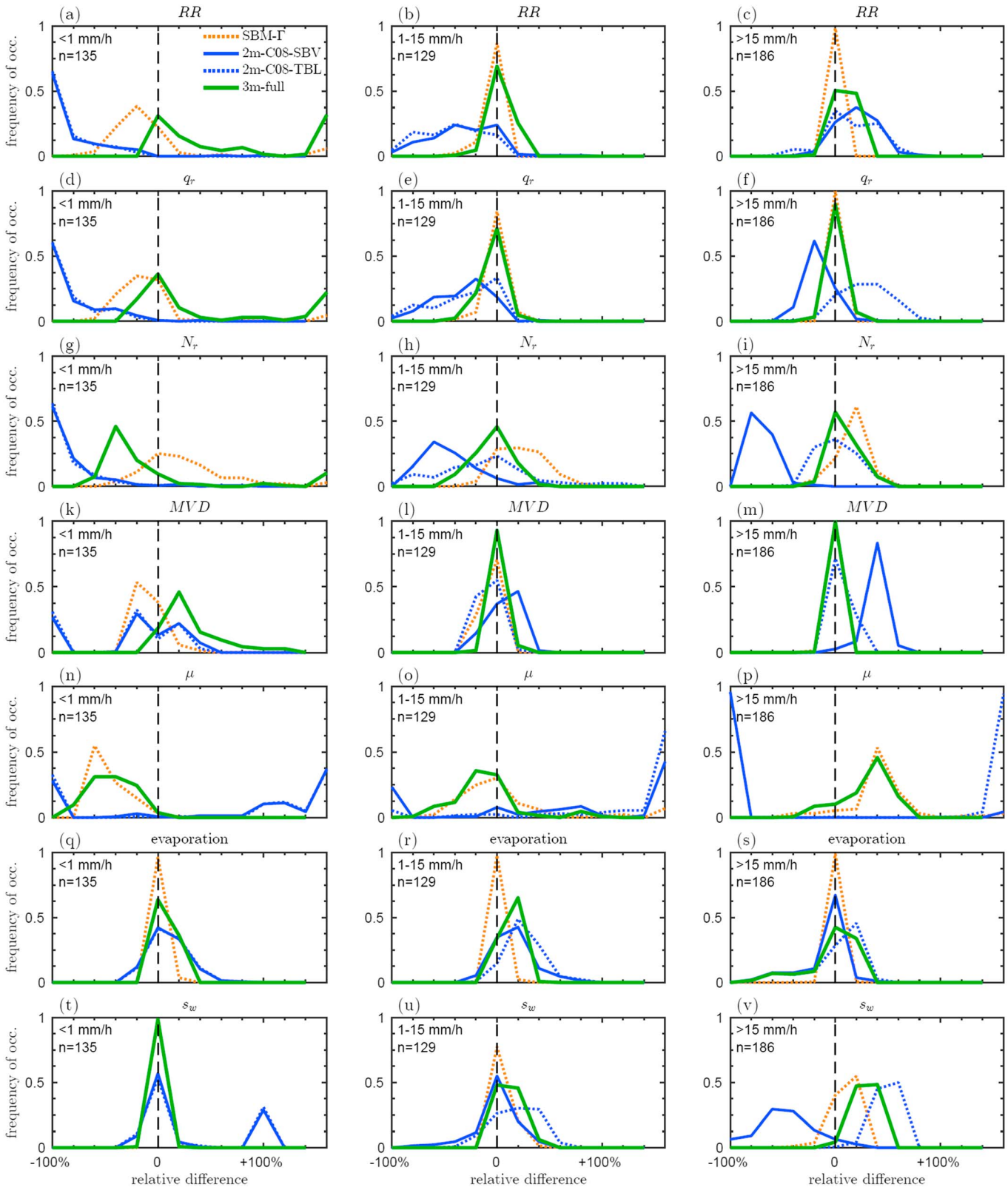

Figure 6. Occurrence frequencies of relative errors compared to Spectral-Bin Model. Rows display rain rate (RR), rain mass mixing ratio (q_r), number mixing ratio (N_r), mean volume diameter (MVD), drop size distribution shape (μ), vertically integrated evaporation rate and supersaturation with respect to water at the surface (s_w). Columns show results for minor to light rain (left, 135 simulations), intermediate rain (middle, 129 simulations), and heavy rain (right 186 simulations). The lines of SBM-Γ are hidden behind 3m-full in panels (m) and (t). Binning is the same as described in Figure 5.

Table 3
Simulations Used to Calculate the Process Contributions as Shown in Figure 4b

Description	Configuration 1	Configuration 2
RSCB mean size effect (3m-S)	3m-S-SBV	3m-S-TBL
RSCB mean size effect (3m-SE)	3m-SE-SBV	3m-SE-TBL
RSCB mean size effect (2m-C08)	2m-C08-SBV	2m-C08-TBL
predicted μ (sedimentation)	2m-C08-TBL	3m-S-TBL
predicted μ (evaporation)	3m-S-TBL	3m-SE-TBL
predicted μ (RSCB)	3m-SE-TBL	3m-full

Note. RSCB = rain self-collection and collisional breakup.

surface rain rates and mean sizes. Remaining differences between 3m-full and the SBM results are further addressed in sections 4.2.4 and 4.2.5.

4.2.2. Important Processes Affecting the Shape Parameter

Generally, an increasing degree of complexity leads to a better agreement with SBM (Figure 4a). Compared to 2m-C08-SBV, 3m-S-SBV yields relatively small improvements. This could be interpreted as an indication that the effect of sedimentation on DSD shape is small. However, because our performance measure also includes variations in mean size, which is highly dependent on the parameterization approach of RSCB, it is more appropriate to compare 3m-S-TBL versus 2m-C08-TBL, rather than 3m-S-SBV versus 2m-C08-SBV, when quantifying the sedimentation effect. In this case, we do find a dominant effect of sedimentation on the predicted shape for rain rates larger than 1 mm/hr (Table 3 and Figure 4b). Further replacing the assumption of constant μ during evaporation with the calculation of physically based rates of M_6 from evaporation (3m-SE-SBV versus 3m-S-SBV) indicates a nonnegligible contribution particularly in the light rain regime. The 3m-full, compared to 3m-SE-TBL, additionally considers the effect of RSCB on the shape parameter. The impact is comparable to the evaporation effect for intermediate rain rates (Figure 4b) and increases with rain intensity. Thus, in the intermediate rain regime, the environmental relative humidity determines whether evaporation or RSCB is more important in affecting the DSD shape.

In Figure 5 it is seen that 3m-S-SBV—where μ is only determined by sedimentation—has a tail of underpredicted rain rates in conjunction with a positive bias of D_n, indicating too narrow DSDs. This is because size sorting by sedimentation pushes μ solely towards large values. 3m-SE-SBV—in which evaporation counteracts the sedimentation effect on DSD shape—helps to mitigate this bias. The effect of RSCB on the shape parameter is visible from comparing 3m-SE-TBL and 3m-full. The main difference is the narrower peak of 3m-full in the distribution of D_n (Figure 5f), indicating a more accurate prediction of the DSD shape.

4.2.3. Effect of RSCB Parameterizations

While there are still mean size biases in the three-moment configurations with the default treatment of RSCB, the new lookup table approach yields considerable improvement for intermediate to heavy rain conditions. In Figure 4a, this is seen by comparing 3m-S-TBL with 3m-S-SBV as well as 3m-SE-TBL with 3m-SE-SBV, corresponding to black dotted and dashed lines in Figure 4b. Figures 5e and 5f confirm that the parameterization of RSCB plays a major role in determining the mean drop sizes, typically reducing them compared to the default P3 scheme.

Using the RSCB lookup table in the two-moment scheme gives only a small improvement (2m-C08-TBL versus 2m-C08-SBV), and the changes are most pronounced in the intermediate rain regime (blue dotted line in Figure 4a and black solid line in Figure 4b). Even though the mean sizes are closer to SBM when using the RSCB lookup table, rain rates are rather insensitive to the parameterization of RSCB in the two-moment configuration (Figures 5a and 5b); thus, performance is not improved when measured by both mean sizes and rain rates.

4.2.4. Effect of Gamma Size Distributions

When forcing the DSD to be consistent with a gamma distribution in SBM (SBM-Γ), the behavior is generally similar to 3m-full. In Figure 4a we see that the fraction of similar runs decreases in the regimes of small rain rates, that is, the ±20% criterion is fulfilled in only 50% (light rain) and 30% (minor rain) of the simulations, respectively. This implies that (a) the assumed gamma DSD degrades the simulation results particularly in simulations of drizzling conditions and (b) in the regimes of small rain rates, a large part of the deviation between 3m-full and SBM originates from the assumed gamma DSD, rather than from the parameterizations used in the bulk scheme.

While there is only 30% similarity between SBM-Γ and SBM in minor rain (see above), this result is still significantly better than 3m-full ($RR < 0.1$ mm/hr in Figure 4a). Because both SBM-Γ and 3m-full show very similar biases in simulated shape parameters compared to the original SBM (Figures 6n–6p), the

differences between SBM-Γ and 3m-full must originate from details other than the DSD shape. Figure 6a reveals underpredicted rain rates in SBM-Γ, but overpredicted rain rates in 3m-full, which is in agreement with the mean drop size biases (Figure 6k). Figures 6d and 6g indicate that number biases may be more dominant in determining mean sizes than mass biases. An important aspect is that the number budget of rain is influenced by evaporation, in addition to RSCB. As described in section 4.2.5, the evaporation effect in P3 tends to deplete too many raindrops, thus creating too large mean sizes. This can also act as a compensating error in P3; for example, in Figure 4a the 3m-full configuration seems to perform better than SBM-Γ in light to intermediate rain. As seen in Figures 6h and 6l, the more efficient raindrop depletion compensates for the error associated with the gamma DSD and thus yields better mean sizes than SBM-Γ (both compared to the freely evolving, original SBM).

4.2.5. Role of Evaporation

Raindrop evaporation is a major remaining source of uncertainty in the 3m-full configuration. One aspect is the estimated number of drops depleted by evaporation, relying on the assumption of MVD being constant during evaporation. Seifert (2008) showed that this assumption may be acceptable for broad DSDs ($\mu \approx 0$), while for narrower DSDs the fraction of drops depleted by evaporation should be smaller than in cases of broad DSDs (thereby reducing MVD during evaporation). This is particularly relevant to lighter rain, where μ can be considerably larger than 0. This may be directly related to the increased mean size described in section 4.2.4. To test this hypothesis, we ran sensitivity simulations in which the constant-*MVD* assumption was replaced by equation (23) of Seifert (2008) and variations of it (e.g., equation (A21) of Naumann & Seifert, 2016), parameterizing the dependency of number rates on the DSD shape (not shown). These tests confirm the general sensitivity of our results to the parameterized number rate depending on μ and also the conclusion of Seifert (2008) that the complicated behavior of this process is difficult to capture by a simple formulation. The tests also showed that the tail of overpredicted rain rates in 3m-full simulations (Figure 6a) is sensitive to this treatment.

Another aspect of evaporation is the loss of bulk mass. Figures 6q–6s show the vertically integrated evaporation rates. Larger rain evaporation rates in P3 result in a moister atmosphere, shown in Figures 6t–6v, which is more pronounced in heavy rain. The efficiency of evaporation is modulated by both MVD and μ. For example, with smaller mean sizes in 2m-C08-TBL (compared to 2m-C08-SBV), the evaporation efficiency is significantly increased in intermediate to heavy rain. In addition to the mean size effect on evaporation, the effect of the diagnosed shape in two-moment configurations is evident particularly in the heavy rain regime (Figures 6p and 6v). While DSDs that are too broad result in reduced evaporation and drier air, narrower DSDs give increased moisture. The different DSD shapes between the two-moment configurations arise because the diagnosed shape indirectly depends on MVD, with smaller MVD corresponding to narrower DSDs.

The 3m-full configuration tends to produce moister air than SBM, particularly in heavy rain (Figure 6v). These differences in mass evaporation rates must be caused by the different evaporation parameterizations, and/or the gamma DSD assumed in P3. Therefore, we next discuss the comparison of 3m-full and SBM-Γ. Figures 6n–6p show that the biases of μ relative to SBM are similar in both schemes, while 3m-full still yields larger evaporation rates compared to SBM-Γ (Figures 6q–6v). Therefore, the gamma DSD as such is unlikely the reason for different evaporation behavior between 3m-full and SBM-Γ. For $RR < 1$ mm/hr, the MVD in 3m-full is too large, which partially compensates the evaporation bias, that is, with the correct mean size, evaporation would be even more biased. Similar arguments apply to the intermediate rain regime in which both mass and number tend to be smaller in 3m-full compared to SBM-Γ. This implies that most of the differences in atmospheric moistening between 3m-full and SBM are owing to the evaporation parameterization itself, rather than the gamma distribution assumption.

5. Conclusions and Discussion

We have developed a three-moment bulk parameterization for rain by prognosing the zeroth (number), third (proportional to mass), and sixth (proportional to reflectivity) moments of the gamma distribution and implemented it in the P3 microphysics scheme. Furthermore, we have developed new formulations for RSCB using a lookup table approach based on the SBM. Accounting for the impact of RSCB on the shape parameter is a unique aspect of this three-moment scheme, and also the effect of evaporation on the shape

parameter has been either treated in a simpler way or neglected in existing three-moment schemes. Our model developments were tested in a 1-D rain shaft model, and we assessed the contribution of each modified process to the model improvements. The following summarizes key points:

1. By predicting the DSD shape in the three-moment rain representation, the agreement between P3 and SBM improves substantially. The dominant processes in determining the shape parameter are evaporation and sedimentation. In heavy rain, RSCB also contributes significantly to the evolution of the shape parameter.
2. The new lookup table parameterization of RSCB makes major contributions to improve the agreement of P3 with SBM. This is owing to impacts on the raindrop number mixing ratios, and thus drop mean sizes, which are smaller compared to the default parameterization. However, applying the new approach for RSCB in the two-moment P3 yields rather small benefits, because in spite of improved mean sizes, the diagnosed shape parameter still yields discrepancies with SBM in the simulated rain rates.
3. Remaining differences in simulations using the new three-moment rain scheme and SBM are attributable to two aspects. First, the evaporation parameterizations are different. P3 assumes a constant mean volume diameter during evaporation, which contributes to overestimated mean sizes particularly in light rain. In addition to the bulk number, the evaporation efficiency for mass is generally higher in P3 compared to SBM. Second, the assumed gamma distribution yields good results in heavy rain but introduces biases in simulations of light rain, compared to a freely evolving DSD in SBM.

While substantial improvement of simulated rain properties with our most advanced three-moment configuration of P3 relative to SBM is encouraging, we suggest possibilities to further enhance the scheme. A more general formulation for the number of drops lost upon complete evaporation would be superior to the assumption of a constant MVD during evaporation. We also have not addressed the initiation of rain, for example, the bulk parameterization of autoconversion is known to be highly uncertain. Because the representation of RSCB using lookup tables was shown to be beneficial for collisional processes in P3, similar approaches might be used in the future for collisional growth that involves cloud droplets. This would also allow the impact of autoconversion and accretion to explicitly affect the shape of rain DSDs.

It may be expected that using the lookup table approach for RSCB in P3 leads to results more similar to SBM, since the tables are based on the physics of SBM. However, we have also shown that even if all microphysical processes are formulated exactly in the same way, that is, comparing the freely evolving SBM to the bulk-emulating bin model (SBM-Γ), assuming a gamma DSD leads to different results, particularly in light rain. These differences may also be related to the particular choice of prognostic moments (e.g., Milbrandt & McTaggart-Cowan, 2010), which was not addressed here. On the other hand, the good agreement between the 3m-full and SBM-Γ configurations can be regarded as proof of concept for the lookup table approach.

Here we used SBM as a benchmark in our comparisons, yet it should be kept in mind that SBM is only an approximation of nature and hence itself has uncertainties. The primary benefit of spectral bin models is that they freely evolve DSDs without a priori assumptions about the DSD form. Although it was shown that different assumptions about the physical properties of ice particles can introduce large uncertainties in both bulk and bin schemes (Xue et al., 2017), this type of uncertainty is minimal in the current study because the properties of liquid drops are well defined. It is also known that numerical treatments can cause artificial DSD broadening in bin schemes. For the SBM scheme used here, a remapping procedure was developed to minimize this effect, which was shown to reproduce observations (Khain et al., 2008). Nevertheless, it should be noted that the knowledge of breakup kernels is imperfect, and so is the representation of collisional breakup in models (Barros et al., 2008; Seifert et al., 2005; Straub et al., 2010).

In addition to the results discussed here, we are testing the new implementation with 3-D real-case simulations of drizzling stratocumulus clouds to confirm its positive impact. Previous studies have pointed out large sensitivities of simulated squall lines to the rain microphysics parameterization (e.g., Feng et al., 2018; Morrison et al., 2012). In future work we will examine the impacts of our three-moment rain scheme on the properties and evolution of a simulated mesoscale squall line system. Because rain originates from the melting of ice particles in many cloud systems, it is our plan to

merge the three-moment rain scheme with ongoing developments of a three-moment ice microphysics scheme in P3 to provide a full three-moment scheme for weather and climate modeling.

Appendix A: Lookup Tables of Rain Self-Collection and Collisional Breakup (RSCB)

Here we discuss the procedure for creating the lookup tables for RSCB. The 33-bin version of SBM solves the quasi-stochastic collection equation for 33 mass-doubling bins, and the breakup scheme follows Seifert et al. (2005). Similar approaches based on bin microphysics were previously introduced for two-moment schemes (e.g., Feingold et al., 1998; Saleeby et al., 2015).

We seek instantaneous RSCB rates for the bulk scheme, and thus only one time step is used by SBM to calculate each lookup table value. Time steps are 1-s long, and the specified pressure is 1,000 hPa. While the collisional growth of cloud droplets was shown to depend on pressure (Pinsky et al., 2001), for raindrops this is considered negligible. Each SBM calculation is initialized with a three-parameter gamma DSD. Bulk RSCB rates for a wide range of DSDs are produced by spanning all relevant combinations of DSD parameters. Here we include the full dependencies on all parameters including the DSD shape; by normalizing the DSDs as described below, we can use only two dimensions in the lookup table (μ and D_n) while implicitly representing variability of all three parameters of the gamma distribution. The rates, representative for a particular DSD, are subsequently stored in lookup tables: $\text{table}_{Nr}(\mu, D_n)$ for bulk number and $\text{table}_{M6}(\mu, D_n)$ for the sixth moment. Mass is conserved during RSCB. The scaling approach is described below. Primed f', N_0', and N_r' are quantities used during lookup table creation with units different from P3 (see Appendix C).

We start from $f'(D) = N_0' D^{\mu} e^{-\lambda D}$ and use the relation $N_0' = N_r' \lambda^{\mu+1}/\Gamma(\mu+1)$ to give

$$f'(D) = \frac{N_r'}{\Gamma(\mu+1)} \lambda^{\mu+1} D^{\mu} e^{-\lambda D} \tag{A1}$$

By normalizing equation (A1) with the factor $N_r'/\Gamma(\mu+1)$, we obtain $f'^*(D)$, which only depends on λ and μ:

$$f'^*(D) = \lambda^{\mu+1} D^{\mu} e^{-\lambda D} \tag{A2}$$

With $\lambda = (\mu+1)/D_n$ (equation (B2)), the normalized size distribution is only a function of the table dimensions, μ and D_n. In principle, SBM can be initialized with $f'^*(D)$ to derive the lookup tables (see below for the method used in practice). As a result of the DSD scaling, values stored in the lookup tables are not equal to the process rates. To obtain the rates in P3 at model runtime, quantities obtained from interpolation of the lookup table values are rescaled using the factor

$$f_{\text{scale}} = \left(\frac{\rho_{\text{air}} N_r}{\Gamma(\mu+1)} \right)^2 \tag{A3}$$

where ρ_{air}, N_r, and μ are the local values at a given time and grid location during the run. f_{scale} is the squared factor which was used to normalize $f'(D)$. This is required by the nature of the stochastic coagulation-breakup equation (equation (7) of Seifert et al., 2005), where each integral contains multiplications of the form $f'(D_1) \times f'(D_2)$, thus yielding a quadratic normalization factor.

In practice, the procedure during lookup table creation is slightly different; rather than using $f'^*(D)$ (equation (A2)) for the process calculations in SBM, $f'(D)$ (equation (A1)) is used to compute the processes. The resulting bulk process rates are then divided by $\left(\frac{N_r'}{\Gamma(\mu+1)}\right)^2$ (corresponding to f_{scale} within the SBM scheme) before storing them in the table. This is found to be numerically more convenient in SBM because $f'^*(D)$ can be orders of magnitude smaller than $f'(D)$. Using equation (A1) in SBM requires knowledge of N_r' which is calculated assuming a constant rain mass concentration of 1 g/m^3 in all calculations. Using this scaling method, the lookup table values do not depend on the specific choice of mass concentration.

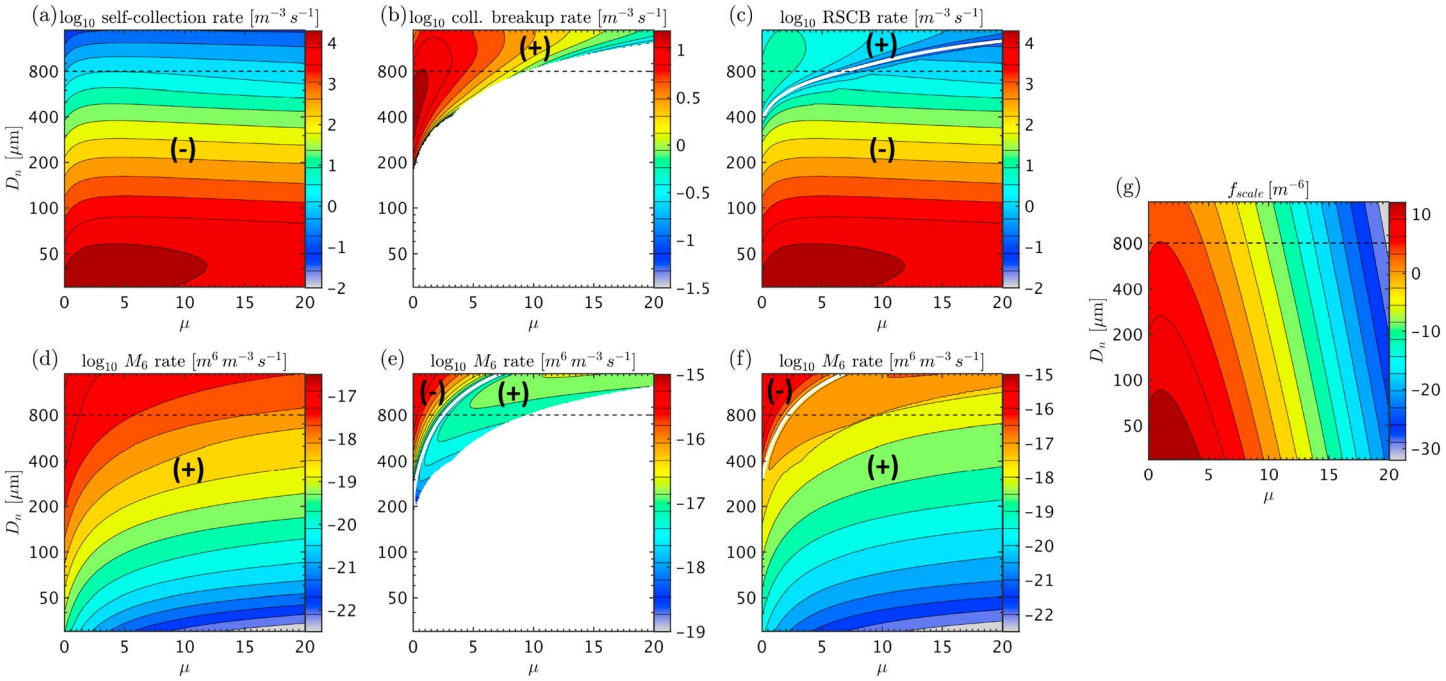

Figure A1. Process rates of number (top panels) and M_6 (bottom panels) derived from the SBM scheme when initialized with gamma DSDs in the space of lookup table dimensions D_n and μ for a rain mass concentration of 1 g/m^3. The color scale represents the base 10 logarithm of the rates. (a and d) Rain self-collection and (b and e) collisional breakup. RSCB (c, f) is the sum of the two processes (i.e., c = a + b and f = d + e). The rates may have both signs which are indicated by (+) and (−) and white lines correspond to a value of 0. (g) The scaling factor as used in equation (10). Dashed lines at D_n = 800 μm indicate the upper size limit allowed in P3. RSCB = rain self-collection and collisional breakup; DSDs = drop size distributions.

Figure A1 displays an example of RSCB rates from the rescaled tables (equation (10)) with a bulk rain mass of 1 g/m^3 throughout the table space. The top panels of Figure A1 show the bulk number rates, and bottom panels show the rates of M_6. The processes of self-collection and collisional breakup are treated separately in SBM, shown in columns 1 and 2 of Figure A1. For convenience in the P3 scheme, these two contributions are combined into one table, that is, the RSCB table (column 3 of Figure A1) is the sum of columns 1 and 2. Figure A1g shows the scaling factor f_{scale} for the same rain mass concentration. Note that because we use a constant bulk mass throughout the table, there are more raindrops present for small mean sizes compared to large ones, which explains the tendency for larger self-collection rates at smaller mean sizes.

The two-dimensional tables contain 201 and 90 elements along the μ and D_n dimensions, respectively. While the interpolation could in principle allow for a coarser spacing, it is particularly important to resolve the steep gradients where the tables transition from positive to negative values, mainly relevant for broad DSDs (white lines in Figures A1c and A1f). The μ dimension is spaced equidistant, whereas every value of D_n is 1.05 times larger than its smaller neighbor.

It is a fundamental property of RSCB to form an equilibrium DSD after a sufficient amount of time (e.g., Hu & Srivastava, 1995). Based on the tables, the equilibrium properties are given by the point in which the zero lines of Figures A1c and A1f would cross each other, at $\mu \approx 0.6$ and $D_n \approx 470$ μm, corresponding to MVD ≈ 724 μm (equation (B3)). These equilibrium properties are different from those described by Seifert (2008), where $\mu \approx 1$ and MVD ≈ 1,100 μm ($D_n \approx 763$ μm) in equilibrium state. This can be related to (a) the different resolution of the DSD grids (33 here versus 130 spectral bins in Seifert, 2008), which was found to be an important factor in determining equilibrium DSDs (Seifert et al., 2005), and (b) the true equilibrium DSD does not exactly match a gamma DSD. In the presence of other processes, mean sizes can be larger than in equilibrium state.

Spontaneous breakup of raindrops (rather than collisional breakup) is currently not included in P3 because the upper limit of rain mean size in P3 is D_n = 800 μm (MVD ≤ 1,454 μm). When creating lookup tables for

spontaneous breakup in a similar manner as described above, we find that this process is comparably unimportant for these mean sizes. Based on Srivastava (1971), this process would only be significant for single-drop sizes of several millimeters. For example, when $\mu = 0$, the bulk number rate of spontaneous breakup becomes comparable to collisional breakup around $D_n = 1{,}100$ μm. At larger sizes around $D_n = 1{,}600$ μm for $\mu = 0$, the rate would be around 10 times larger. Spontaneous breakup is expected to be relevant mainly in the presence of melting ice particles, which can initiate comparably large raindrops. In contrast, during growth by collision-coalescence, collisional breakup would act as a limiting factor with equilibrium sizes smaller than $D_n = 800$ μm. In a follow-on study of convective rain, we will explore whether the simulated rain properties are sensitive to the currently used upper mean size limit, versus applying explicit spontaneous breakup with a less restrictive limit.

Appendix B: Measures of Drop Mean Size

Here we introduce two measures of the mean raindrop size that are used throughout the paper. Depending on bulk mass and bulk number, the mean volume diameter is defined by

$$\mathrm{MVD} = \left(\frac{q_r}{N_r}\frac{6}{\pi\rho_w}\right)^{\frac{1}{3}} \tag{B1}$$

following, for example, Szyrmer et al. (2005). The number-weighted mean size is defined by

$$D_n = \frac{M_1}{M_0} = \frac{\mu+1}{\lambda} \tag{B2}$$

Using the relation $\lambda = \left(\frac{\pi\rho_w}{6}\frac{N_r}{q_r}\frac{\Gamma(\mu+4)}{\Gamma(\mu+1)}\right)^{\frac{1}{3}}$, the number-weighted mean size can also be expressed in terms of MVD and μ,

$$D_n = \mathrm{MVD}\, g(\mu) \tag{B3}$$

$$g(\mu) = (\mu+1)\left[(\mu+3)(\mu+2)(\mu+1)\right]^{-\frac{1}{3}} \tag{B4}$$

The dimensionless $g(\mu)$ ranges from approximately 0.55 ($\mu = 0$) up to 0.96 ($\mu = 20$) and approaches 1.0 for monodisperse raindrops. Thus, for a given bulk mass and number, D_n increases for narrower DSDs.

Appendix C: List of Symbols

Symbol	Unit	Description
c, c_1, c_2, c_3	1	Coefficients
d	1	Exponent
D	m	Drop diameter
D_n	m	Number-weighted drop mean size
D_v	m^2/s	Diffusivity of water vapor in air
$f(D)$	$kg^{-1}\ m^{-1}$	Drop number size distribution
$f'(D)$	m^{-4}	Drop number size distribution
$f'^*(D)$	m^{-1}	Scaled drop number size distribution
f_{scale}	m^{-6}	Scaling factor
f_p	1	Psychrometric factor
f_v	1	Ventilation factor
$g(\mu)$	1	Function that relates *MVD* and D_n
K	1	Substitution
m	kg	Single-drop mass
M_k	$m^k\ kg^{-1}$	kth moment of $f(D)$
MVD	m	Mean volume diameter
N_0	$m^{-\mu-1}\ kg^{-1}$	Intercept of $f(D)$
N_0'	$m^{-\mu-4}$	Intercept of $f'(D)$

N_r	kg^{-1}	Rain bulk number mixing ratio
N_r'	m^{-3}	Rain bulk number concentration
q_r	kg kg^{-1}	Rain bulk mass mixing ratio
RR	mm hr	Surface rain rate
Sc	1	Schmidt number
t	s	Time
$table_{Nr}$	m^3 s^{-1}	Lookup table value for bulk number
$table_{M6}$	m^9 s^{-1}	Lookup table value for M_6
$v(D)$	ms^{-1}	Single-drop fall speed
V_k	ms^{-1}	M_k-weighted fall speed
z	m	Altitude
$\bar{\delta}$	kg kg^{-1}	Time step-averaged absolute supersaturation
Γ	1	Complete gamma function
λ	m^{-1}	Slope of $f(D)$
μ	1	Shape of $f(D)$
μ_{air}	kg m^{-1} s^{-1}	Dynamic viscosity of air
ρ_{air}	kg m^3	Density of air
ρ_w	kg m^3	Density of liquid water

Acknowledgments
This research was supported by the Climate Model Development and Validation program funded by the Office of Biological and Environmental Research in the U.S. Department of Energy Office of Science. Model simulations were performed using PNNL Institutional Computing at Pacific Northwest National Laboratory. The Pacific Northwest National Laboratory (PNNL) is operated for the DOE by Battelle Memorial Institute under contract DE-AC05-76RL01830. The standard P3 model code is contained in the official release of the WRF model, and the three-moment scheme may be released at a later point. Model output is available at http://portal.nersc.gov/project/m2689/p3. We thank Axel Seifert for helpful discussions about the breakup scheme and Hui Wan, Anshu Dubey, and Balwinder Singh for software help.

References

Atlas, D., & Ulbrich, C. (2006). Drop size spectra and integral remote sensing parameters in the transition from convective to stratiform rain. *Geophysical Research Letters*, *33*, LI6803. https://doi.org/10.1029/2006GL026824

Barros, A. P., Prat, O. P., Shrestha, P., Testik, F. Y., & Bliven, L. F. (2008). Revisiting Low and List (1982): Evaluation of raindrop collision parameterizations using laboratory observations and modeling. *Journal of the Atmospheric Sciences*, *65*(9), 2983–2993. https://doi.org/10.1175/2008jas2630.1

Brandes, E. A., Zhang, G., & Vivekanandan, J. (2003). An evaluation of a drop distribution–based polarimetric radar rainfall estimator. *Journal of Applied Meteorology*, *42*(5), 652–660. https://doi.org/10.1175/1520-0450(2003)042<0652:aeoadd>2.0.co;2

Brdar, S., & Seifert, A. (2018). McSnow: A Monte-Carlo particle model for riming and aggregation of ice particles in a multidimensional microphysical phase space. *Journal of Advances in Modeling Earth Systems*, *10*, 187–206. https://doi.org/10.1002/2017ms001167

Bringi, V. N., Chandrasekar, V., Hubbert, J., Gorgucci, E., Randeu, W. L., & Schoenhuber, M. (2003). Raindrop size distribution in different climatic regimes from disdrometer and dual-polarized radar analysis. *Journal of the Atmospheric Sciences*, *60*(2), 354–365. https://doi.org/10.1175/1520-0469(2003)060<0354:rsdidc>2.0.co;2

Cao, Q., Zhang, G., Brandes, E., Schuur, T., Ryzhkov, A., & Ikeda, K. (2008). Analysis of video disdrometer and polarimetric radar data to characterize rain microphysics in Oklahoma. *Journal of Applied Meteorology and Climatology*, *47*(8), 2238–2255. https://doi.org/10.1175/2008jamc1732.1

Chosson, F., Vaillancourt, P. A., Milbrandt, J. A., Yau, M. K., & Zadra, A. (2014). Adapting two-moment microphysics schemes across model resolutions: Subgrid cloud and precipitation fraction and microphysical sub–time step. *Journal of the Atmospheric Sciences*, *71*(7), 2635–2653. https://doi.org/10.1175/jas-d-13-0367.1

Dawson, D. T. II, Mansell, E. R., Jung, Y., Wicker, L. J., Kumjian, M. R., & Xue, M. (2014). Low-level Z_{DR} signatures in supercell forward flanks: The role of size sorting and melting of hail. *Journal of the Atmospheric Sciences*, *71*(1), 276–299. https://doi.org/10.1175/jas-d-13-0118.1

Dolan, B., Fuchs, B., Rutledge, S. A., Barnes, E. A., & Thompson, E. J. (2018). Primary modes of global drop size distributions. *Journal of the Atmospheric Sciences*, *75*(5), 1453–1476. https://doi.org/10.1175/jas-d-17-0242.1

Feingold, G., Walko, R. L., Stevens, B., & Cotton, W. R. (1998). Simulations of marine stratocumulus using a new microphysical parameterization scheme. *Atmospheric Research*, *47-48*, 505–528. https://doi.org/10.1016/s0169-8095(98)00058-1

Feng, Z., Leung, L. R., Houze, R. A. Jr., Hagos, S., Hardin, J., Yang, Q., Han, B., et al. (2018). Structure and evolution of mesoscale convective systems: Sensitivity to cloud microphysics in convection-permitting simulations over the United States. *Journal of Advances in Modeling Earth Systems*, *10*, 1470–1494. https://doi.org/10.1029/2018ms001305

Forbes, R., Jakob, C., & Miller, M. (2015). Numerical models: Parameterization of physical processes. In *Encyclopedia of Atmospheric Sciences* (pp. 187–193). Elsevier. https://doi.org/10.1016/b978-0-12-382225-3.00307-8

Hu, Z., & Srivastava, R. C. (1995). Evolution of raindrop size distribution by coalescence, breakup, and evaporation: Theory and observations. *Journal of the Atmospheric Sciences*, *52*(10), 1761–1783. https://doi.org/10.1175/1520-0469(1995)052<1761:eorsdb>2.0.co;2

Igel, A. L., & van den Heever, S. C. (2017). The importance of the shape of cloud droplet size distributions in shallow cumulus clouds. Part II: Bulk microphysics simulations. *Journal of the Atmospheric Sciences*, *74*(1), 259–273. https://doi.org/10.1175/jas-d-15-0383.1

Khain, A., Pokrovsky, A., Pinsky, M., Seifert, A., & Phillips, V. (2004). Simulation of effects of atmospheric aerosols on deep turbulent convective clouds using a spectral microphysics mixed-phase cumulus cloud model. Part I: Model description and possible applications. *Journal of the Atmospheric Sciences*, *61*(24), 2963–2982. https://doi.org/10.1175/jas-3350.1

Khain, A. P., Beheng, K. D., Heymsfield, A., Korolev, A., Krichak, S. O., Levin, Z., Pinsky, M., et al. (2015). Representation of microphysical processes in cloud-resolving models: Spectral (bin) microphysics versus bulk parameterization. *Reviews of Geophysics*, *53*, 247–322. https://doi.org/10.1002/2014rg000468

Khain, A. P., BenMoshe, N., & Pokrovsky, A. (2008). Factors determining the impact of aerosols on surface precipitation from clouds: An attempt at classification. *Journal of the Atmospheric Sciences*, *65*(6), 1721–1748. https://doi.org/10.1175/2007jas2515.1

Kumjian, M. R., & Ryzhkov, A. V. (2010). The impact of evaporation on polarimetric characteristics of rain: Theoretical model and practical implications. *Journal of Applied Meteorology and Climatology*, *49*(6), 1247–1267. https://doi.org/10.1175/2010jamc2243.1>

Lim, K.-S. S., & Hong, S.-Y. (2010). Development of an effective double-moment cloud microphysics scheme with prognostic cloud condensation nuclei (CCN) for weather and climate models. *Monthly Weather Review*, *138*(5), 1587–1612. https://doi.org/10.1175/2009mwr2968.1

Lin, Y.-L., Farley, R. D., & Orville, H. D. (1983). Bulk parameterization of the snow field in a cloud model. *Journal of Climate and Applied Meteorology*, *22*(6), 1065–1092. https://doi.org/10.1175/1520-0450(1983)022<1065:bpotsf>2.0.co;2

List, R., & McFarquhar, G. M. (1990). The evolution of three-peak raindrop size distributions in one-dimensional shaft models. Part I: Single-pulse rain. *Journal of the Atmospheric Sciences*, *47*(24), 2996–3006. https://doi.org/10.1175/1520-0469(1990)047<2996:teotpr>2.0.co;2

Loftus, A. M., Cotton, W. R., & Carrió, G. G. (2014). A triple-moment hail bulk microphysics scheme. Part I: Description and initial evaluation. *Atmospheric Research*, *149*, 35–57. https://doi.org/10.1016/j.atmosres.2014.05.013

Marshall, J. S., & Palmer, W. M. K. (1948). The distribution of raindrops with size. *Journal of Meteorology*, *5*(4), 165–166. https://doi.org/10.1175/1520-0469(1948)005<0165:tdorws>2.0.co;2

Milbrandt, J. A., & McTaggart-Cowan, R. (2010). Sedimentation-induced errors in bulk microphysics schemes. *Journal of the Atmospheric Sciences*, *67*(12), 3931–3948. https://doi.org/10.1175/2010jas3541.1

Milbrandt, J. A., & Morrison, H. (2016). Parameterization of cloud microphysics based on the prediction of bulk ice particle properties. Part III: Introduction of multiple free categories. *Journal of the Atmospheric Sciences*, *73*(3), 975–995. https://doi.org/10.1175/jas-d-15-0204.1

Milbrandt, J. A., Thériault, J., & Mo, R. (2012). Modeling the phase transition associated with melting snow in a 1D kinematic framework: Sensitivity to the microphysics. *Pure and Applied Geophysics*, *171*(1–2), 303–322. https://doi.org/10.1007/s00024-012-0552-y

Milbrandt, J. A., & Yau, M. K. (2005a). A multimoment bulk microphysics parameterization. Part I: Analysis of the role of the spectral shape parameter. *Journal of the Atmospheric Sciences*, *62*(9), 3051–3064. https://doi.org/10.1175/jas3534.1

Milbrandt, J. A., & Yau, M. K. (2005b). A multimoment bulk microphysics parameterization. Part II: A proposed three-moment closure and scheme description. *Journal of the Atmospheric Sciences*, *62*(9), 3065–3081. https://doi.org/10.1175/jas3535.1

Morrison, H., Curry, J. A., & Khvorostyanov, V. I. (2005). A new double-moment microphysics parameterization for application in cloud and climate models. Part I: Description. *Journal of the Atmospheric Sciences*, *62*(6), 1665–1677. https://doi.org/10.1175/jas3446.1

Morrison, H., & Grabowski, W. W. (2008). Modeling supersaturation and subgrid-scale mixing with two-moment bulk warm microphysics. *Journal of the Atmospheric Sciences*, *65*(3), 792–812. https://doi.org/10.1175/2007jas2374.1

Morrison, H., Jensen, A. A., Harrington, J. Y., & Milbrandt, J. A. (2016). Advection of coupled hydrometeor quantities in bulk cloud microphysics schemes. *Monthly Weather Review*, *144*(8), 2809–2829. https://doi.org/10.1175/mwr-d-15-0368.1

Morrison, H., & Milbrandt, J. A. (2015). Parameterization of cloud microphysics based on the prediction of bulk ice particle properties. Part I: Scheme description and idealized tests. *Journal of the Atmospheric Sciences*, *72*(1), 287–311. https://doi.org/10.1175/jas-d-14-0065.1

Morrison, H., Milbrandt, J. A., Bryan, G. H., Ikeda, K., Tessendorf, S. A., & Thompson, G. (2015). Parameterization of cloud microphysics based on the prediction of bulk ice particle properties. Part II: Case study comparisons with observations and other schemes. *Journal of the Atmospheric Sciences*, *72*(1), 312–339. https://doi.org/10.1175/jas-d-14-0066.1

Morrison, H., Tessendorf, S. A., Ikeda, K., & Thompson, G. (2012). Sensitivity of a simulated midlatitude squall line to parameterization of raindrop breakup. *Monthly Weather Review*, *140*(8), 2437–2460. https://doi.org/10.1175/mwr-d-11-00283.1

Morrison, H., Thompson, G., & Tatarskii, V. (2009). Impact of cloud microphysics on the development of trailing stratiform precipitation in a simulated squall line: Comparison of one- and two-moment schemes. *Monthly Weather Review*, *137*(3), 991–1007. https://doi.org/10.1175/2008mwr2556.1

Naumann, A. K., & Seifert, A. (2016). Evolution of the shape of the raindrop size distribution in simulated shallow cumulus. *Journal of the Atmospheric Sciences*, *73*(6), 2279–2297. https://doi.org/10.1175/jas-d-15-0263.1

Pinsky, M., Khain, A., & Shapiro, M. (2001). Collision efficiency of drops in a wide range of Reynolds numbers: Effects of pressure on spectrum evolution. *Journal of the Atmospheric Sciences*, *58*(7), 742–764. https://doi.org/10.1175/1520-0469(2001)058<0742:ceodia>2.0.co;2

Press, W. H., Teukolsky, S. A., Vetterling, W. T., & Flannery, B. P. (1992). Numerical recipes in FORTRAN. In *The art of scientific computing* (2nd ed., pp. 179–180). New York: Cambridge University Press.

Saleeby, S. M., Herbener, S. R., van den Heever, S. C., & L'Ecuyer, T. (2015). Impacts of cloud droplet–nucleating aerosols on shallow tropical convection. *Journal of the Atmospheric Sciences*, *72*(4), 1369–1385. https://doi.org/10.1175/jas-d-14-0153.1

Seifert, A. (2005). On the shape–slope relation of drop size distributions in convective rain. *Journal of Applied Meteorology*, *44*(7), 1146–1151. https://doi.org/10.1175/jam2254.1

Seifert, A. (2008). On the parameterization of evaporation of raindrops as simulated by a one-dimensional rainshaft model. *Journal of the Atmospheric Sciences*, *65*(11), 3608–3619. https://doi.org/10.1175/2008jas2586.1

Seifert, A., & Beheng, K. D. (2001). A double-moment parameterization for simulating autoconversion, accretion and self-collection. *Atmospheric Research*, *59-60*, 265–281. https://doi.org/10.1016/s0169-8095(01)00126-0

Seifert, A., & Beheng, K. D. (2006). A two-moment cloud microphysics parameterization for mixed-phase clouds. Part 1: Model description. *Meteorology and Atmospheric Physics*, *92*(1–2), 45–66. https://doi.org/10.1007/s00703-005-0112-4

Seifert, A., Khain, A., Blahak, U., & Beheng, K. D. (2005). Possible effects of collisional breakup on mixed-phase deep convection simulated by a spectral (bin) cloud model. *Journal of the Atmospheric Sciences*, *62*(6), 1917–1931. https://doi.org/10.1175/jas3432.1

Shipway, B. J., & Hill, A. A. (2012). Diagnosis of systematic differences between multiple parametrizations of warm rain microphysics using a kinematic framework. *Quarterly Journal of the Royal Meteorological Society*, *138*(669), 2196–2211. https://doi.org/10.1002/qj.1913

Srivastava, R. C. (1971). Size distribution of raindrops generated by their breakup and coalescence. *Journal of the Atmospheric Sciences*, *28*(3), 410–415. https://doi.org/10.1175/1520-0469(1971)028<0410:sdorgb>2.0.co;2

Straub, W., Beheng, K. D., Seifert, A., Schlottke, J., & Weigand, B. (2010). Numerical investigation of collision-induced breakup of raindrops. Part II: Parameterizations of coalescence efficiencies and fragment size distributions. *Journal of the Atmospheric Sciences*, *67*(3), 576–588. https://doi.org/10.1175/2009jas3175.1

Szyrmer, W., Laroche, S., & Zawadzki, I. (2005). A microphysical bulk formulation based on scaling normalization of the particle size distribution. Part I: Description. *Journal of the Atmospheric Sciences*, *62*(12), 4206–4221. https://doi.org/10.1175/jas3620.1

Ulbrich, C. W. (1983). Natural variations in the analytical form of the raindrop size distribution. *Journal of Climate and Applied Meteorology*, *22*(10), 1764–1775. https://doi.org/10.1175/1520-0450(1983)022<1764:nvitaf>2.0.co;2

Ulbrich, C. W., & Atlas, D. (2007). Microphysics of raindrop size spectra: Tropical continental and maritime storms. *Journal of Applied Meteorology and Climatology*, *46*(11), 1777–1791. https://doi.org/10.1175/2007jamc1649.1

Verlinde, J., & Cotton, W. R. (1993). Fitting microphysical observations of nonsteady convective clouds to a numerical model: An application of the Adjoint technique of data assimilation to a kinematic model. *Monthly Weather Review*, *121*(10), 2776–2793. https://doi.org/10.1175/1520-0493(1993)121<2776:fmoonc>2.0.co;2

Wacker, U., & Seifert, A. (2001). Evolution of rain water profiles resulting from pure sedimentation: Spectral vs. parameterized description. *Atmospheric Research*, *58*(1), 19–39. https://doi.org/10.1016/s0169-8095(01)00081-3

Waugh, S. M., Ziegler, C. L., & MacGorman, D. R. (2018). In situ microphysical observations of the 29–30 May 2012 Kingfisher, OK, supercell with a balloon-borne video disdrometer. *Journal of Geophysical Research: Atmospheres*, *123*, 5618–5640. https://doi.org/10.1029/2017JD027623

Wisner, C., Orville, H. D., & Myers, C. (1972). A numerical model of a hail-bearing cloud. *Journal of the Atmospheric Sciences*, *29*(6), 1160–1181. https://doi.org/10.1175/1520-0469(1972)029<1160:anmoah>2.0.co;2

Xie, S., Lin, W., Rasch, P. J., Ma, P.-L., Neale, R., Larson, V. E., Qian, Y., et al. (2018). Understanding cloud and convective characteristics in version 1 of the E3SM atmosphere model. *Journal of Advances in Modeling Earth Systems*, *10*, 2618–2644. https://doi.org/10.1029/2018ms001350

Xue, L., Fan, J., Lebo, Z. J., Wu, W., Morrison, H., Grabowski, W. W., Chu, X., et al. (2017). Idealized simulations of a squall line from the MC3E field campaign applying three bin microphysics schemes: Dynamic and thermodynamic structure. *Monthly Weather Review*, *145*(12), 4789–4812. https://doi.org/10.1175/mwr-d-16-0385.1

Zhang, G., Vivekanandan, J., & Brandes, E. (2001). A method for estimating rain rate and drop size distribution from polarimetric radar measurements. *IEEE Transactions on Geoscience and Remote Sensing*, *39*(4), 830–841. https://doi.org/10.1109/36.917906

Zhang, K., Rasch, P. J., Taylor, M. A., Wan, H., Leung, R., Ma, P.-L., Golaz, J. C., et al. (2018). Impact of numerical choices on water conservation in the E3SM Atmosphere Model version 1 (EAMv1). *Geoscientific Model Development*, *11*(5), 1971–1988. https://doi.org/10.5194/gmd-11-1971-2018

Ziemer, C., & Wacker, U. (2014). A comparative study of *B*-, Γ- and log-normal distributions in a three-moment parameterization for drop sedimentation. *Atmosphere*, *5*(3), 484–517. https://doi.org/10.3390/atmos5030484